JOURNAL OF CATALYSIS 138, 115–128 (1992)

The Effect of Nonframework Aluminum on Acidity in Dealuminated Mordenite

J. T. MILLER,*,[1] P. D. HOPKINS,* B. L. MEYERS,† G. J. RAY,† R. T. ROGINSKI,† G. W. ZAJAC,† AND N. H. ROSENBAUM†

Amoco Oil Company, P. O. Box 3011, H-4, Naperville, Illinois 60566-7011; and †Amoco Corporation, Analytical Research and Services Division, P. O. Box 3011, Naperville, Illinois 60566-7011

Received October 8, 1991; revised June 15, 1992

Despite its high crystalline stability, mordenite (MOR) is relatively easily dealuminated. Calcination of NH_4–MOR to H–MOR at 500°C results in 20% dealumination with the production of octahedral, nonstructural aluminum located within the zeolite pores. The octahedral aluminum is nonacidic and does not affect the acid strength of the remaining structural aluminum ions. Calcination at 735°C results in over 50% dealumination, creating internal, nonacidic pentacoordinate aluminum. In H–MOR (735), 60% of the acid sites are equivalent in strength to H–MOR (500); however, the remaining acid sites are reduced in strength. Pentacoordinated aluminum may interact with the portion of structural aluminum, reducing their acid strength. Dealumination by strong acid removes 75% of the structural aluminum; the aluminum is completely removed from the mordenite, leaving no nonframework species. Strong acid creates many SiOH defect sites; however, the SiOH defects did not affect the acid strength. High-temperature steam produces extensive dealumination. In the presence of steam, nonstructural aluminum migrates to the crystallite surface and restricts the pore aperture. Eventually, the pore aperture becomes sufficiently restricted that large molecules, e.g., *n*-hexane or pyridine, cannot diffuse to the zeolite interior. In steam-dealuminated mordenite, pentacoordinate aluminum also reduces the acid strength of 40% of the remaining acid sites. Qualitatively, the catalysts' activities for hexane cracking could be correctly ordered by either the number of strong acid sites (independent of the maximum acid strength) measured by NH_3 TPD or infrared spectroscopy. © 1992 Academic Press, Inc.

INTRODUCTION

Significant progress has been made in recent years in understanding the factors affecting zeolite acidity. Theoretical (*1–3*) and experimental (*4–6*) evidence indicates that the distribution of framework aluminum ions is a critical factor in the development of acid strength. The maximum in Brønsted acid strength per aluminum occurs when the framework aluminum ions have no second-nearest neighbor aluminum (*4–6*).

In addition to acid strength, several studies have demonstrated that catalytic activity increases in direct proportion to the number of strong Brønsted acid sites (*7–11*). For example, in Y zeolite, the maximum of strong Brønsted acid sites, i.e., isolated framework aluminum ions, occurs at 32 Al/unit cell. Catalytic activity for hexane (*4*), isobutane (*11*), and cumene (*5, 9*) cracking increases linearly with increasing framework aluminum up to 32 Al/unit cell. Similarly, in ZSM-5, the catalytic activity for hexane cracking increases linearly with increasing structural aluminum (*7, 8*).

For reactions requiring strong acid sites, catalytic activity parallels the number of Brønsted acid sites (*5, 7, 12*). There appears to be little evidence for the contribution of Lewis acidity in paraffin cracking activity in HY, ZSM-5, or silica–alumina catalysts (*13*).

In several zeolites, the existence of enhanced, or super-acidic, acid sites has been demonstrated (*4, 5, 11, 14–21*). In each case, superacidity is associated with the presence

[1] To whom correspondence should be addressed.

0021-9517/92 $5.00
Copyright © 1992 by Academic Press, Inc.
All rights of reproduction in any form reserved.

of extra framework aluminum in addition to isolated framework aluminum ions. Several explanations have been proposed to explain the origin of the super-acid site. In H–Y, one explanation suggests that the strength of the framework Brønsted sites is increased by the generation of Lewis sites associated with extraframework aluminum (*11*). An alternative explanation suggests that super-acid sites are due to the presence of amorphous silica–alumina inside the pores formed during dealumination (*20*). A third proposal suggests that a portion of the nonstructural aluminum is located in the sodalite cages of H–Y. The extraframework polyvalent aluminum-oxide species in the sodalite cages withdraw electrons from the framework hydroxyl groups, making the framework Brønsted sites more acidic (*4, 5*).

Super-acid sites for paraffin cracking have also been confirmed for ZSM-5 following mild steaming (*16–19*). One explanation proposes that two paired aluminum ions, i.e., an aluminum with a second-nearest neighbor aluminum, is modified during steaming, perhaps being partially hydrolyzed. The modified (nonstructural) aluminum thus acts as an electron withdrawing group enhancing the acidity of the aluminum pair (*16*). An alternative model suggests that the reacting molecules simultaneously react with the Brønsted acid sites and nonframework aluminum Lewis acid centers. This model requires a balance of structural and extraframework aluminum for optimum activity (*17, 18*).

Finally, a maximum in activity for hexane cracking occurs for mordenite dealuminated with dilute acid (*21*). Alternatively, very strong acid sites may be developed in mordenite following steaming at 500°C (*14, 15*). In both studies, the enhanced acid strength or catalytic activity was accompanied by the formation of nonframework Lewis acid sites. For acid dealuminated mordenite, the Lewis acid was thought to dehydrogenate paraffins to olefins (*21*). On the other hand, for steam-dealuminated mordenite, the Lewis acid was thought to bridge to the structural hydroxyl acid site, withdrawing electron density and increasing the acid strength of the structural Brønsted hydroxyl group (*14*).

In this study, mordenite was dealuminated by low- and high-temperature (dry) heating, strong acid, and steam. The number of acid sites was determined by infrared spectroscopy and temperature-programmed desorption of ammonia, NH_3 TPD. The strength of the acid sites was determined by NH_3 TPD, while the type of acid site, Lewis or Brønsted, was determined by infrared spectroscopy after pyridine adsorption. The type of aluminum species, e.g., tetrahedral, pentacoordinate, or octahedral, has been identified by Al NMR. The location of extraframework aluminum ions was determined by XPS and Xe NMR. For several dealuminated mordenites, the nonstructural aluminum species were observed to modify the acid strength of the remaining structural acid sites. Finally, the effect of catalyst acidity was related to the catalysts' hexane cracking activity.

EXPERIMENTAL

Catalyst Preparation

A commercially available ammonium-exchanged mordenite, obtained from Conteka BV, was used as the starting material. H-mordenite catalysts were prepared by calcination at 500°C, 735°C (dry) calcination, steam (650°C and 1 atm steam) treatment, or acid (6*N* HCl) treatment. Steam and acid treated samples were subsequently calcined at 500°C. The catalyst treatments, aluminum analysis, and XRD crystallinity are listed in Table 1. All H–mordenite catalysts had less than 10 ppm Na.

n-Hexane Cracking

Hexane cracking was performed using an integral, fixed-bed, gas-phase, plug-flow reactor equipped with an on-line gas chromatograph. The experimental apparatus and procedures were similar to those previously described (*22, 23*). The zeolites were cal-

TABLE 1

Catalyst Treatment, Aluminum Elemental Analysis, and Crystallinity

Catalyst	Treatment	%Al	%Crystallinity[a]
NH_4–MOR	None	3.79	98
H–MOR (500)	500°C/2 hr	3.69	92
H–MOR (735)	735°C/6 hr	3.72	78
H–MOR (HCl)	6 N HCl (100°C)/3 hr	0.73	81
H–MOR (steam)	Steam (1 atm, 650°C)/24 hr	3.86	71

[a] Crystallinity determined by XRD.

cined at 550°C before testing. *n*-Hexane was introduced in a nitrogen stream saturated at 0°C, and the conversion was measured 5 min after the start of the hexane flow.

Analytical Methods

Standard procedures were used for analyses of catalysts for surface area, micropore volume, elemental analysis, X-ray diffraction (XRD), Si and Al NMR, as well as electron spectroscopy for chemical analysis (XPS) (*24*).

Temperature programmed desorption (TPD) of ammonia was conducted in standard equipment. Ammonia was adsorbed at 200°C and desorbed by temperature programming at 10 C/min to 700°C under an He flow rate of 20 cc/min. The desorbed NH_3 was trapped in a buffer solution and maintained at constant pH of 5.0 with 0.01 *N* HCl added from an automatic titrator. Preliminary analysis of each mordenite determined the number of acid sites per gram of catalyst. Subsequently, peak temperatures were determined by adjusting the sample size such that the amount of NH_3 desorbed above 200°C was identical for each catalyst. The TPD spectra were deconvoluted with SpectraCalc software from Galactic Industries (Salem, New Hampshire). The peak shapes were assumed to be Gaussian (*25*).

Infrared samples were prepared as 0.15-g pressed disks with a diameter of 3.2 cm. Each sample was evacuated to 10^{-4} Torr at room temperature and further dried under vacuum at 300°C. The sample was cooled to room temperature and a background spectrum was obtained. At room temperature, the sample was dosed with 3 Torr of pyridine for 5 min. The excess pyridine was removed by heating the sample to 100°C for 30 min under vacuum. Infrared spectra were obtained at room temperature on a Nicolet 6000C Fourier transform infrared spectrometer equipped with a high-sensitivity MCT/InSb detector. Spectra were acquired from 3450–3850 cm^{-1}, e.g., the hydroxyl region, and from 1200–1800 cm^{-1} for adsorbed pyridine.

Xe NMR samples were prepared in special NMR tubes (Wilmad Corporation) equipped with a resealable valve suitable for attachment to a vacuum line. The sample was evacuated (10^{-3} Torr) for 1 h at ambient temperature, followed by evacuation overnight at 200°C. ^{129}Xe NMR spectra were obtained at ambient temperature on an NT300 spectrometer at a frequency of 83.0 MHz using simple pulse-acquire-delay sequences. The spectral width was 16 kHz. Data were acquired into 1k blocks of memory, but were zero-filled to 4k to enhance digital resolution to 0.1 ppm. Delay times were 500 msec. Generally, 1200 scans were acquired for each sample. Referencing of chemical shifts was made relative to the gas at infinite dilution. ^{129}Xe NMR spectra were obtained at 30, 60, 100, 150, 200, 300, 400, and 500 Torr.

Adsorption of hexane and mesitylene were performed on a modified DuPont TGA apparatus (*26*) and in a constant-volume, constant-pressure Cahn balance. Measurements were conducted at 100°C.

RESULTS AND DISCUSSION

H–mordenite, H–MOR (500), was prepared by deammination of NH_4–mordenite, NH_4–MOR, by heating at 500°C for 2 h in flowing air. Subsequently, H–MOR (500) was dealuminated by either 735°C dry calcination for 6 h, 6 *N* HCl reflux for 3 h, or 650°C steaming for 24 h. For each catalyst, the nature, i.e., the strength, number, and type of acid sites, was characterized

by NH_3 TPD, infrared spectroscopy, and hexane cracking. In addition, the structure and location of the aluminum species were determined by XPS, Si, Al, and Xe NMR.

n-Hexane Cracking

Cracking of *n*-hexane has been a useful tool for characterizing strong acidity of zeolite since the introduction of the alpha test (*27, 28*). The relative ranking for *n*-hexane cracking was determined by the temperature required for 25% conversion, T_{25}. The relative hexane cracking activities decrease from H–MOR (500) [T_{25} = 235°C] > H–MOR (735) [T_{25} = 322°C] > H–MOR (HCl) [T_{25} = 366°C] > H–MOR (steam) [T_{25} = 595°C].

Si and Al NMR

The use of ^{29}Si NMR to determine the framework Si/Al ratio is well established (*29*). However, accurate determination of this ratio is not always possible in highly dealuminated zeolites, since the peaks associated with framework aluminum become small and difficult to measure. In addition, the peak due to silanol sites has a chemical shift that overlaps the shift of the Si(1 Al) peak. Therefore, in more highly dealuminated zeolites, the intensity from silanol defects makes a significantly larger contribution to the intensity of the peak assigned to Si(1 Al). Qualitatively, however, at low aluminum levels, increased dealumination can be monitored by ^{29}Si NMR from the splitting of the Si(0 Al) peak into several resonances.

The ^{29}Si NMR spectrum, Fig. 1a, of NH_4–MOR consists of two broad peaks corresponding to Si(1 Al) and Si(0 Al) at −108 and −113 ppm (*30, 31*), respectively. The spectrum of H–MOR (500), Fig. 1b, is similar to that of NH_4–MOR except that the −108-ppm peak is about half as intense. This indicates that partial framework dealumination has occurred. Treatment of H–MOR (500) with 6 *N* HCl, i.e., H–MOR (HCl), results in a large decrease in the −108 ppm resonance. In addition, the splitting of the −113-ppm peak, Fig. 1c, indicates extensive dealumination. For H–MOR (735) significant dealumination is indicated by the very weak −108-ppm peak and the partial resolution of the −113-ppm peak, Fig. 1d. Steaming at 650°C for 24 h results in the most highly dealuminated zeolite. In the spectrum of H–MOR (steam), Fig. 1e, the −108-ppm peak due to Si(1 Al) is no longer visible and the peak at −113 ppm has been clearly split into three peaks at −112.9, −113.7, and −115.3 ppm. Mordenite has crystallographically nonequivalent tetrahedral sites with a relative ratio of 1 : 1 : 2 : 2. The three peaks in the spectrum of H–MOR (steam) are due to these four sites with the relative intensities of 2 : 1 : 3 caused by an overlap of one peak with intensity 1 and one peak with intensity 2. The excellent resolution of these three resonances is an indication that this is the most highly dealuminated catalyst.

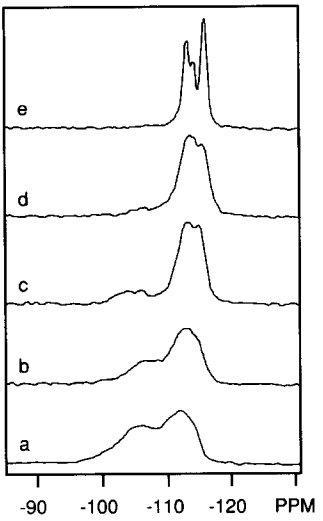

FIG. 1. ^{29}Si NMR: (a) NH_4–MOR, (b) H–MOR (500), (c) H–MOR (HCl), (d) H–MOR (735), (e) H–MOR (steam).

Additional information is provided by the cross-polarization (CP) ^{29}Si NMR (*31–33*). This technique depends on the dipolar coupling of a silicon with a proton and transfer of magnetization from the protons to the

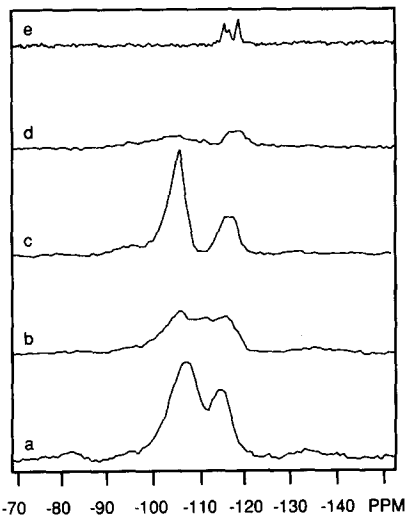

FIG. 2. CP ^{29}Si NMR: (a) NH_4–MOR, (b) H–MOR (500), (c) H–MOR (HCl), (d) H–MOR (735), (e) H–MOR (steam).

silicons. Because the efficiency of the cross-polarization has an r^{-3} dependence, the relative intensity of a given silicon peak will depend on its proximity to a proton. Therefore, silanols will have much more intense peaks than silicons distant from these defect sites. The dependence of the silicon intensity on the distance to a proton means that CP data are inherently nonquantitative. However, a relative comparison of the CP spectra is possible if CP spectra are obtained on samples pretreated and run identically.

The CP spectrum of NH_4–MOR, Fig. 2a, has two very intense peaks at -105 and -113 ppm. Because this zeolite is in the ammonium ion form and relatively high in aluminum content, most of the intensity is attributed to Si(1 Al) and Si(0 Al) sites near to ammonium ions. Note the -105-ppm peak is more intense than the -113-ppm peak, a reversal of the peak intensities observed in the Bloch decay (BD) spectrum, Fig. 1a, and is an indication that many of the Si(0 Al) sites are too distant from the ammonium ions for cross-polarization. The Si(1 Al) peak at -105 ppm in the CP spectrum is shifted from -108 ppm in the BD spectrum, indicating that there is a large contribution from SiOH groups to this peak in the CP spectrum. The CP spectrum of H–MOR (500), Fig. 2b, also shows significant intensity in the Si(1 Al) peak due to the large number of protons, i.e., acid sites, associated with these aluminums. Although H–MOR (HCl) has fewer acid sites, there is a relatively more intense band at -102 ppm, Fig. 2c. This large -102-ppm resonance is due to silonol defects created by acid dealumination (*34*). These defects are present despite calcination of the catalyst at 500°C. The spectra of H–MOR (735), Fig. 2d, and H–MOR (steam), Fig. 2e, appear to have few silonol groups. Thus, acid dealumination results in a large number of SiOH defect sites, while thermal or steam dealumination results in few silonol defects.

The Al NMR spectrum of NH_4–MOR mordenite consists of one sharp resonance at 55 ppm which is assigned to structural, tetrahedral aluminum (*35*), Fig. 3a. The Al spectrum of H–MOR (500), Fig. 3b, has two peaks: one at 55 ppm and 0 ppm. As observed for NH_4–MOR, the peak at 55 ppm is relatively sharp and is assigned to structural, tetrahedral Al. The peak at 0 ppm is assigned to nonstructural, octahedral aluminum (*36*). Calcination at 500°C, e.g.,

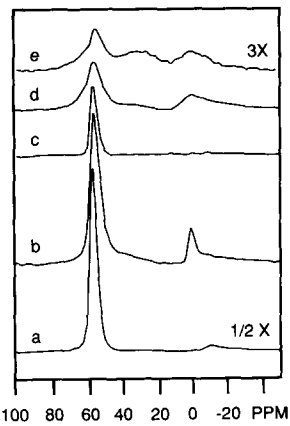

FIG. 3. ^{27}Al NMR: (a) NH_4–MOR, (b) H–MOR (500), (c) H–MOR (HCl), (d) H–MOR (735), (e) H–MOR (steam).

TABLE 2

^{27}Al NMR

Catalyst	%Al NMR Intensities			Structural %Al[a]
	55 ppm (Tetrahedral)	30 ppm (Pentacoordinate)	0 ppm (Octahedral)	
NH_4–MOR	100	0	0	3.79
H–MOR (500)	80	0	20	2.94
H–MOR (735)	37	36	27	1.39
H–MOR (HCl)	100	0	0	0.73
H–MOR (steam)	22	60	18	0.75

[a] Structural %Al = %Al (elemental analysis) × %Al NMR (55 ppm)/100.

H–MOR (500), results in approximately 20% dealumination, Table 2. Concentrated HCl treatment of H–MOR (500) removes approximately 75% of the structural aluminum and completely removes the nonframework, octahedral Al, i.e., the 0-ppm resonance, Fig. 3c. The Al NMR spectrum of H–MOR (735) indicates that high-temperature calcination causes extensive framework dealumination, Fig. 3d. In addition to the 55-ppm tetrahedral and 0-ppm octahedral peaks, a new resonance appears near 30 ppm. The 30-ppm peak is often assigned to pentacoordinate, nonstructural aluminum oxide (*37*). A further feature of the spectrum is the broadness of all of the peaks. Although one might expect line broadening due to structural disorder for peaks associated with amorphous aluminum oxides, i.e., octahedral and pentacoordinate aluminum, one would not expect a broad distribution of aluminum environments for crystalline, tetrahedral aluminum. It is possible, therefore, that a portion of the intensity of the 55-ppm in H–MOR (735) is nonstructural tetrahedral aluminum (*38, 39*). Amorphous tetrahedral aluminum with a resonance at 55 ppm has been reported in silica–alumina (*40*). In any case, H–MOR (735) contains, at least, three different aluminum oxide species. The relative amounts of tetrahedral, pentacoordinate, and octahedral aluminum, determined by Al NMR are given in Table 2. Pentacoordinate aluminum, as well as tetrahedral and octahedral aluminum, is also present in H–MOR (steam), Fig. 3e. As much as 60% of the aluminum in H–MOR (steam) is pentacoordinate with an additional 18% associated with nonstructural octahedral aluminum sites.

Although high-temperature steaming has resulted in extensive structural dealumination of mordenite, steam has produced much less damage to the crystalline structure as evidenced by the XRD crystallinity, Table 1. For example, while over 80% of the structural aluminum is lost upon steaming, the crystallinity of H–MOR (steam) is 71% compared with a crystallinity of 92% for H–MOR (500).

Although different aluminum species are readily identified by Al NMR, quantitative determination of the various aluminum species is poor since much of the signal is lost during the spectrometer recovery time immediately after the application of the excitation pulse. This has lead to reports of "NMR-invisible aluminum" (*41*). In order to estimate the percent aluminum for each signal, each peak is assumed to contribute equally to the NMR spectrum. The fractional intensity is then multiplied by the wt% aluminum determined by elemental analysis to estimate the amount of that aluminum. The estimates of structural aluminum by NMR for these mordenites is given in Table 2. The amount of tetrahedral aluminum by Al NMR will overestimate the amount of

structural aluminum if nonstructural, tetrahedral aluminum is present.

In summary, both Si and Al NMR indicate that the various treatments result in increased dealumination in the order from 500°C calcination < 735°C calcination < strong acid < steaming. In addition to the differences in the number of structural aluminum ions among the H–mordenite catalysts, there are other differences determined by NMR. For example, H–MOR (500) has 20% of the Al in nonstructural, octahedral aluminum coordination. H–MOR (HCl) has a large number of SiOH defect sites; while H–MOR (735) and H–MOR (steam) each have pentacoordinate, as well as octahedral, aluminum. These differences among the H–mordenites could potentially alter the nature of the acid sites which could lead to changes in the catalysts' acid strength and performance.

Infrared Spectroscopy

The frequencies and assignments for adsorbed pyridine are listed below (*42*).

Band assignment, acid type	Band frequency, cm^{-1}
Brønsted	1635
Brønsted + Lewis (predom. Lewis)	1620
H-bonded	1593
Lewis	1580
Brønsted	1550
Brønsted + Lewis	1490
Lewis	1450
H-bonded	1445

The 1550-cm^{-1} band, Brønsted sites (pyridinium ions), and the 1450-cm^{-1} band, Lewis coordinated pyridine, were free from overlap of other absorbances. For mordenites having SiO_2/Al_2O_3 ratios greater than about 12, the ratio of extinction coefficients (Brønsted/Lewis) is about 1.5 (*43, 44*). For each H–mordenite, the relative number of Brønsted, Lewis, and total acid sites is given in Table 3. NH_4–MOR, after evacuation at 300°C, has the greatest number of total acid sites, approximately 83% of which are Brønsted sites. The number of total acid sites decreases approximately 9% in H–MOR (500), while the percentage of Brønsted sites remains high at ca. 85%. The total acidity of H–MOR (735) decreases to 40% that of H–MOR (500). Moreover, over 66% of the pyridine is adsorbed on Lewis acid sites. For H–MOR (HCl), the total acidity is approximately 23% that of H–MOR (500) with over 70% of those Brønsted sites. H–MOR (steam) has very low acidity as determined by pyridine adsorption.

TABLE 3

Infrared Spectroscopy of Adsorbed Pyridine[a]

Catalyst[b]	Brønsted acidity (1550 cm^{-1})	Lewis acidity (1450 cm^{-1})	Total acidity
NH_4–MOR	1.33	0.27	1.60
H–MOR (500)	1.24	0.22	1.46
H–MOR (735)	0.20	0.39	0.59
H–MOR (HCl)	0.25	0.09	0.34
H–MOR (steam)	0.03	0.06	0.09

[a] Values given in relative concentration units.
[b] Catalysts evacuated at 300°C prior to pyridine adsorption.

Hydroxyl region. Several hydroxyl absorptions, in the absence of pyridine, are present in the region from 3400 to 3800 cm^{-1}, Fig. 4. Except for H–MOR (HCl), Fig. 4c, the hydroxyl region for each catalyst is similar. Hydroxyl bands are present at 3780 (weak), 3744 (strong), 3725 (weak), 3685 (weak), 3660 (weak), and 3600 cm^{-1} (variable). The band at 3600 cm^{-1} is acidic and interacts strongly with pyridine. After pyridine adsorption, the 3600 cm^{-1} is no longer observed on H–MOR (500), H–MOR (735), and H–MOR (HCl). For H–MOR (steam), however, the 3600 cm^{-1} does not interact with pyridine. As discussed later, it was determined that large molecules, for example, *n*-hexane and mesitylene, are not adsorbed by H–MOR (steam) due to constriction of the pore aperture. The infrared determination of acidity by pyridine adsorption, therefore, is incorrect for H–MOR (steam) since pyridine could not diffuse into the catalyst.

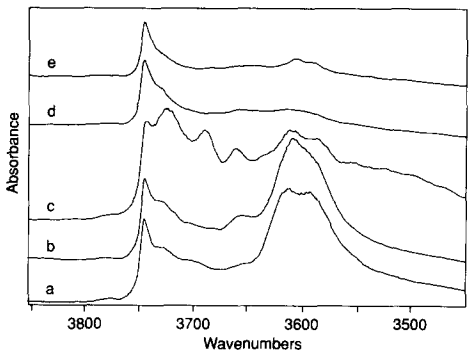

FIG. 4. Infrared spectra (hydroxyl region): (a) NH_4–MOR, (b) H–MOR (500), (c) H–MOR (HCl), (d) H–MOR (735), (e) H–MOR (steam).

Although Brønsted acidity of H–MOR (735) and H–MOR (HCl) differs by less than 25% relative, as determined by the 1550 cm^{-1} band intensity (Table 3), the 3600-cm^{-1} band in H–MOR (HCl) is four times as intense as the corresponding band in H–MOR (735). In addition, the hydroxyl band near 3665 cm^{-1} in H–MOR (HCl) interacts strongly with pyridine and could represent a Brønsted acid site. The 3665 cm^{-1} band in H–MOR (735) is much weaker and is not affected by treatment with pyridine. While detailed assignment of all the bands is not possible, it is clear that the catalysts differ, not only in the number of acid sites, but also in the type of acid sites, i.e., Brønsted or Lewis. H–MOR (HCl) was determined to have many more nonacidic hydroxyl bands, perhaps SiOH defect sites detected by CP Si NMR. Furthermore, in H–MOR (HCl), the existence of a Brønsted acid site with a characteristic hydroxyl frequency at 3665 cm^{-1} was detected which was not present in the other samples.

X-Ray Photoelectron Spectroscopy (XPS)

The surface composition in atomic percent for the mordenite catalysts is given in Table 4 along with the Si/Al atomic ratios determined by both XPS and elemental analysis. The surface aluminum concentration was found to be little changed by calcination for either H–MOR (500) or H–MOR (735). On the other hand, steaming, i.e., H–MOR (steam), increases the surface aluminum content by about a factor of two. Dealumination by strong acid reduces the surface and bulk aluminum concentrations by the same amounts as shown by the comparable Si/Al ratios of surface and bulk compositions. These results suggest that dealumination by (dry) calcination leaves nonstructural aluminum within the pores of the zeolite. Dealumination by steam, by contrast, results in the migration of, at least, a portion of the nonstructural aluminum toward the crystal surface. Strong acid uniformly dealuminates mordenite and removes all nonframework aluminum.

Xe NMR

The room temperature Xe NMR spectra of the H-mordenites and, Na-mordenite (for comparison) are given in Fig. 5. Na–mordenite consists of two peaks, Fig. 5a. The peak at 233 ppm, which is independent of Xe pressure, results from Xe in the smaller, eight-ring pores. By contrast, the low-frequency band which results from Xe adsorbed in the 12-ring large pores is pressure-dependent with the chemical shift decreasing with decreasing pressure (*45*), Fig. 6a. The chemical shift of the low-frequency band extrapolated to zero pressure is 99 ppm. The integrated intensities of the low-frequency and high-frequency bands are 70 and 30%, respectively, of the total area. The Xe NMR spectra of H–MOR (HCl), Fig.

TABLE 4

XPS Surface Composition (Atomic Percent)

Catalyst	Si	Al	C	O	Si/Al[a]	Si/Al[a] (elemental analysis)
H–MOR	31.3	2.4	5.7	63.9	13.0	11.4
H–MOR (500)	28.9	1.9	11.5	57.7	15.2	11.8
H–MOR (735)	29.3	2.0	11.6	56.9	14.7	11.7
H–MOR (HCl)	31.8	0.5	11.7	56.0	63.6	63.0
H–MOR (steam)	25.4	4.5	15.6	54.3	5.6	11.2

[a] Atomic ratio.

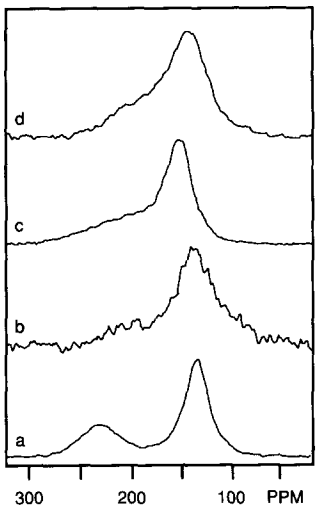

FIG. 5. ^{129}Xe NMR (200 Torr): (a) Na–MOR, (b) H–MOR (HCl), (e) H–MOR (500), (d) H–MOR (735).

5b, also consists of two peaks, although the high-frequency peak is weaker and accounts for only 10–15% of the total intensity. The chemical shift of the larger low-frequency peak decreases with decreasing pressure. Its chemical shift at zero pressure is 128 ppm, Fig. 6b. Since univalent cations have a negligible effect on the chemical shift (*46*), if one assumes that there is free exchange of Xe between the small pore (233 ppm in Na–mordenite) and the large pore (99 ppm in Na–mordenite), then a chemical shift of 128 ppm in H–MOR (HCl) indicates that Xe is in the large pores 78% of the time and in the small pores 22% of the time, in reasonable agreement with the two pore volumes determined for Na–mordenite. Two Xe NMR peaks are observed for H–MOR (500), Fig. 5c. The high-frequency peak at 210 ppm is slightly more intense than observed for H–MOR (HCl). The pressure dependence of the low-frequency (large pore) peak is quite different from that of Na–mordenite and H–MOR (HCl). As the pressure decreases, the chemical shift remains constant and increases slightly at pressures below 100 Torr, Fig. 6c. The chemical shift at zero pressure is estimated to be 164 ppm for H–MOR (500). The increase in chemical shift at low pressures is characteristic of zeolites with highly charged cations (*47*), possibly aluminum (+3), within the large pores. In H–MOR (500), there appear to be at least two contributions to the chemical shift, relative to Na–mordenite. First, there appears to be exchange of Xe between the large and small pores, and second, there appear to be highly charged cations within the large pores, further increasing the chemical shift.

Two peaks are again evident for H–MOR (735). The high-frequency peak is approximately 25% of the total intensity, slightly less than the 30% intensity of the high-frequency peak in Na–mordenite. Unlike Na–mordenite, however, the high-frequency peak, Fig. 5d, is much broader, perhaps indicating that some of the nonstructural aluminum is in the smaller pores. The chemical shift of the low-frequency peak increases with pressure and is consistent with highly charged cations within the large pores. The chemical shift at zero pressure is 155 ppm, Fig. 6d. For H–MOR (735), the increase in chemical shift of the low-frequency peak is evident over a larger pressure range, indicative of larger quantities of nonstructural aluminum, compared with H–MOR (500). In addition, the observed chemical shift in the large pores of H–MOR

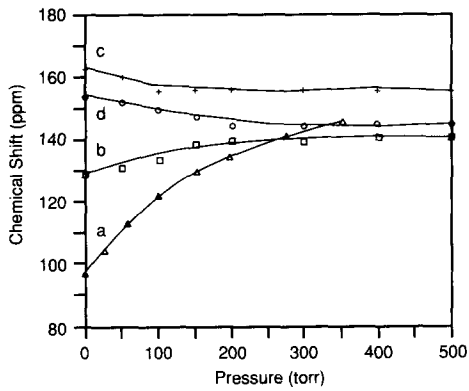

FIG. 6. ^{129}Xe chemical shift of the low-frequency peak vs pressure: (a) Na–MOR, (b) H–MOR (HCl), (c) H–MOR (500), (d) H–MOR (735).

TABLE 5

Porosity and Adsorption of Mordenites

Catalyst	N_2 micropore vol. (cc/g)	Wt% uptake (mesitylene)	Wt% uptake (*n*-hexane)
NH_4-MOR	0.147	—	—
H-MOR (500)	0.194	7.2	4.7
H-MOR (735)	0.170	6.4	4.2
H-MOR (HCl)	0.184	5.4	4.3
H-MOR (steam)	0.146	0.1	0.2

(735) is lower, 155 ppm versus 164 ppm. We speculate that a portion of the nonstructural aluminum in H-MOR (735) is located in the small pores, effectively blocking free exchange of Xe between the large and small pores. With restricted diffusion of Xe, the chemical shift in the large pores is lower, i.e., shifted toward the chemical shift of the large pores in Na-mordenite, 99 ppm. The Xe NMR spectrum of H-MOR (steam) was very weak at all pressures, indicating, at most, trace adsorption of Xe.

In summary, the Xe NMR data indicate that in H-MOR (500), nonstructural aluminum ions or oxides remain internal to the large zeolite pores. In H-MOR (735), greater quantities of nonstructural aluminum are present both in the large and small pores. In H-MOR (735), due to the larger quantities of nonstructural aluminum, diffusion from the large to the small pores is partially restricted. Dealumination by 6 *N* HCl removes nonstructural aluminum. Xe freely diffuses from the larger to the smaller pores. In H-MOR (steam), the large pores are severely restricted, and despite the 71% crystallinity does not adsorb Xe.

Adsorption of Mesitylene and n-Hexane

The amounts of mesitylene and *n*-hexane adsorbed at saturation are listed in Table 5. The initial absorption is rapid followed by a slow approach to saturation. For example, on H-MOR (500) approximately 75% of the mesitylene is rapidly adsorbed in less than 1 min. The remaining mesitylene is more slowly adsorbed, reaching equilibrium in approximately 20 min. For each H-MOR, except H-MOR (steam), the equilibrium amount of mesitylene or *n*-hexane sorbed is proportional to the XRD crystallinity given in Table 1. For H-MOR (steam), however, sorption of both mesitylene and *n*-hexane is very low. By comparison, N_2 micropore volumes of all the H-MOR, also given in Table 5, is proportional to the XRD crystallinity, even for H-MOR (steam). These results indicate that in H-MOR (steam), the micropore volume is accessible to small molecules such as N_2, which has a kinetic diameter of 0.36 nm, but not larger molecules such as mesitylene, *n*-hexane, Xe, or pyridine, which all have kinetic diameters greater than 0.4 nm. It appears that the pore aperture in H-MOR (steam) is smaller than in the other H-mordenites. As shown above by XPS, steaming causes some of the nonframework aluminum to migrate to the crystallite surface. Apparently, however, most of the aluminum remains in the pores, constricting the pore aperture. Despite the high crystallinity and large N_2 micropore volume of H-MOR (steam), the restricted pore aperture prevents diffusion of organic reactants to the zeolite interior.

Temperature-Programmed Desorption of Ammonia

Each catalyst was initially analyzed by TPD to determine the amount of NH_3 desorbed per gram. In subsequent TPDs, the sample weight was adjusted such that the amount of NH_3 desorbed above 200°C was equivalent for each catalyst. At 200°C, weakly physisorbed ammonia is eliminated simplifying the TPD spectra and improving the resolution of the acid sites. The spectra are shown in Fig. 7, and the data are given in Table 6.

NH_4-MOR, H-MOR (500), and H-MOR (HCl) have a single ammonia desorption at 411, 412, and 396°C, respectively. The amount of desorbed ammonia, assuming one ammonia per aluminum, is equivalent to 3.81% Al in NH_4-MOR and 0.90% Al for H-MOR (HCl) in good agreement with the

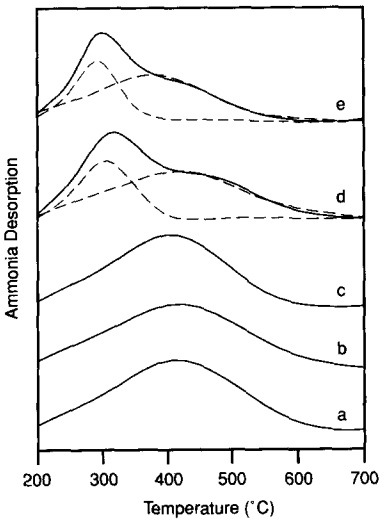

FIG. 7. Temperature-programmed desorption of ammonia: (a) NH_4–MOR, (b) H–MOR (500), (c) H–MOR (HCl), (d) H–MOR (735), (e) H–MOR (steam).

elemental analysis, Table 1. For H–MOR (500), however, the amount of desorbed ammonia corresponds to 3.00% Al, which is less than the aluminum content by elemental analysis, e.g., 3.69%. By contrast, the TPD spectra for H–MOR (735) and H–MOR (steam) require fitting with two peaks. In H–MOR (735), 66% of the acid sites desorb ammonia at 413°C while the remaining acid sites desorb ammonia at lower temperature, 303°C. In H–MOR (steam) 60% of the sites desorb ammonia at 370°C with the remainder of the ammonia desorbed at lower a temperature, 290°C. For both H–MOR (735) and H–MOR (steam) the amount of desorbed ammonia corresponds to 1.16 and 0.26% Al, respectively, which is much less than the aluminum content by elemental analysis; see Table 1. For all catalysts, however, the total amount of Al by TPD agreed closely with the quantity of tetrahedral aluminum by Al NMR. Apparently, only tetrahedral aluminum, i.e., structural aluminum, is acidic. All of the nonstructural aluminum, whether in octahedral or pentacoordination, is nonacidic.

Although the relative acid strengths can be inferred from the peak desorption temperatures if the number of acid sites in each catalyst and the experimental conditions are identical, quantitative determination of the heat of ammonia desorption requires a series of TPD measurements, which vary in, for example, sample size (*48–52*). For NH_4–MOR, the heat of desorption, ΔH, is 154 kJ/mole determined from the slope of $\ln(T_m/W)$ vs $1/T_m$, where T_m is the peak temperature and W is the weight of the catalyst. This value is in good agreement with previous determinations of the heat of ammonia desorption by TPD (*51, 52*). From the experimental ΔH and Eq. (1) (*51, 52*), the entropy of adsorption, ΔS, is 162 J/mole-K in good agreement with previous results (*52*):

$$\ln T_m - \ln A_0 \cdot W/F = \Delta H/RT_m + \ln[B(1-\Theta)^2(\Delta H - RT_m)/P^0 \exp(\Delta S/R)]. \quad (1)$$

TABLE 6
NH_3 TPD of Dealuminated Mordenites

Catalyst	Peak 1			Peak 2			%Al total TPD	%Td Al Al NMR
	%Al	T_m (C)	ΔH (kJ/mole)	%Al	T_m (C)	ΔH (kJ/mole)		
NH_4–MOR	—	—	—	3.73	411	154	3.81	3.79
H–MOR (500)	—	—	—	2.97	412	154	3.00	2.94
H–MOR (735)	0.40	303	134	0.76	413	157	1.16	1.39
H–MOR (HCl)	—	—	—	0.88	396	151	0.90	0.73
H–MOR (steam)	0.092	290	132	0.16	370	148	0.262	0.75

[a] NH_3 adsorption at 200°C.

Assuming a constant ΔS for each mordenite, ΔH can be calculated from a single peak temperature using Eq. (1) (*52*). The heats of ammonia desorption, ΔH, are listed in Table 6. Each of the mordenites have strong acid sites of equivalent strength with ΔH approximately 150 kJ/mole. For H–MOR (735) and H–MOR (steam), however, there is an additional weaker acid site. ΔH for the weaker acid site is ca. 133 kJ/mole.

Comparison of the Al NMR with the TPD indicates that the octahedral aluminum present in H–MOR (500) is nonacidic and does not alter the strength of the remaining acid sites. In H–MOR (HCl) the acid sites are also equivalent in strength to those in NH_4–MOR or H–MOR (500). Neither the aluminum density, nor the presence of large numbers of silonol sites, alters the acid strength. In H–MOR (735) approximately 60% of the acid sites are equivalent in strength to the original NH_4–MOR, while, the remaining 40% of the sites are reduced in strength. Al NMR shows that much of the nonframework aluminum is pentacoordinate and, as evidenced by XPS and Xe NMR, resides within the zeolite pores. It is speculated that the pentacoordinate aluminum may interact with some of the framework acid sites and reduce the acid strength. The acid sites of reduced strength are also present in H–MOR (steam) where pentacoordinate aluminum is also present within the pores.

Relationship between Hexane Cracking and Acidity

Several conclusions can be made with respect to the catalysts' hexane cracking activity. Qualitatively, catalyst activity can be correctly ordered, based on the number of acid sites by TPD or total acidity, Brønsted plus Lewis, determined by infrared spectroscopy of adsorbed pyridine. For example, in H–MOR (735) there are fewer strong acid sites, ΔH = 157 kJ/mole, but more total acid sites than for H–MOR (HCl). Nevertheless, H–MOR (735) with a greater number of acid sites, is more active for hexane cracking than H–MOR (HCl). Hexane cracking activity, therefore, is determined more by the number of acid sites, rather than the strength of the acid sites, at least, when the acid strength is greater than 130 kJ/mol.

Although total infrared acidity correctly ordered the hexane cracking activities, neither Brønsted nor Lewis acidity alone correctly ordered the catalyst activities. For example, H–MOR (HCl) had more Brønsted acidity than H–MOR (735), but was less active. Similarly, H–MOR (735) had more Lewis acidity than H–MOR (500), but was much less active. While Brønsted and Lewis acid sites may not be equally effective for paraffin cracking, both types of acid sites must contribute to the cracking activity.

CONCLUSIONS

Mordenite is known as a zeolite of high stability that maintains high crystallinity even after severe treatment by strong acid, high temperature, or steam. While the crystalline structure is stable, dealumination occurs under relatively mild conditions. For example, in NH_4–MOR, 20% of the aluminum is lost from the structure following calcination at 500°C to produce H–mordenite. Calcination at 735°C results in over 50% dealumination. By contrast, a similar 735°C, dry calcination of H–USY (unit cell dimension = 2.454 nm) resulted in no loss of structural aluminum.

In the presence of steam, nonstructural aluminum in mordenite migrates toward the crystallite surface as has been reported by H–USY (*53*). In contrast to HY (*54*), there is less migration of the nonstructural aluminum to the crystallite surface in mordenite, with much of the aluminum remaining internal to the pores. At high levels of dealumination by steam, all pores became sufficiently restricted to prohibit diffusion of reactant molecules to the zeolite interior. While nonstructural aluminum is mobile in the presence of steam, nonstructural aluminum pro-

duced by high-temperature (dry) calcination is immobile and remains inside the zeolite pores.

None of the nonstructural aluminum produced by the different methods of dealumination is acidic. When present in low concentration, as in H–MOR (500), the nonstructural (octahedral) aluminum has no effect on the acid strength of the remaining structural aluminum. However, when large amounts of nonstructural, pentacoordinate aluminum are present in the pores of the zeolite, the acid strength of many of the acid sites is decreased. The pentacoordinate aluminum oxide species may interact with a portion of the remaining structural aluminum reducing their acid strength. While large amounts of pentacoordinate aluminum decrease the acid strength of some acid sites, silonol defects (SiOH) created by strong acid dealumination have no effect on the acid strength.

Although the mordenites studied differ widely in the number, strength, and type of acid sites, qualitatively, there is a correlation between the catalytic reactivity and the number of acid sites. Acid sites with an enthalpy of absorbtion (for ammonia) greater than 130 kJ/mole appear to contribute to the cracking activity. The number of acid sites for hexane cracking could be determined by either Al NMR, NH_3 TPD, or infrared spectroscopy. While the hexane cracking activity depends on the number of strong acid sites, both the acid strength and the type of acid site, Brønsted or Lewis, appears to be less important for hexane cracking.

REFERENCES

1. Dempsey, E., *J. Catal.* **33,** 497 (1974).
2. Dempsey, E., *J. Catal.* **39,** 155 (1975).
3. Mikovsky, R. J., and Marshall, J. F., *J. Catal.* **44,** 170 (1976).
4. Carvajal, R., Chu, P.-J., and Lunsford, J. H., *J. Catal.* **125,** 123 (1990).
5. Lunsford, J. H., *Prepr. Am. Chem. Soc. Div. Pet. Chem.* **35**(4), 654 (1990).
6. Sawa, M., Niwa, M., and Murakami, Y., *Zeolites* **10,** 532 (1990).
7. Haag, W. O., Lago, R. M., and Weisz, P. B., *Nature* **309,** 989 (1984).
8. Borade, R. B., Hegde, S. G., Kulkarni, S. B., and Ratnasamy, P., *Appl. Catal.* **13,** 27 (1984).
9. De Canio, S. J., Sahn, J. R., Fritz, P. O., and Lunsford, J. H., *J. Catal.* **101,** 132 (1986).
10. Sohn, J. R., De Canio, S. J., Fritz, P. O., and Lunsford, J. H., *J. Phys. Chem.* **90,** 4847 (1986).
11. Beyerlein, R. A., McVicker, G. B., Yacullo, L. N., and Ziemiak, L.N., *J. Phys. Chem.* **92,** 1967 (1988).
12. Ward, J. W., and Hansford, R. C., *J. Catal.* **13,** 364 (1969).
13. Abbot, J., *J. Catal.* **126,** 628 (1990).
14. Mirodatos, C., and Barthomeuf, D., *J. Chem. Soc., Chem. Commun.* 39 (1981).
15. Mirodatos, C., Ha, B. H., Otsuka, and Barthomeuf, D., *in* "Proceedings, Fifth International Conference on Zeolites" (L. V. C. Rees, Ed.), p. 382. Naples, 1980.
16. Lago, R. M., Haag, W. O., Mikovsky, R. J., Olson, D. H., Hellring, S. D., Schmitt, K. D., and Kerr, G. T., *in* "Proceedings, 7th International Zeolite Conference" (Y. Murakami, A. Lyima and J. W. Ward, Eds.), p. 677. Tokyo, 1986.
17. Sendota, Y., and Ono, Y., *Zeolites* **8,** 101 (1988).
18. Brunner, E., Ernst, H., Freude, D., Hunger, M., Krause, C. B., Prager, D., Reschetilowski, W., Schwilger, W., and Bergk, K.-H., *Zeolites* **9,** 282 (1989).
19. Vasques, M. H., Ribeiro, F. R., Gnep, N., and Guisnet, M., *React. Kinet. Catal. Lett.* **38**(2), 301 (1989).
20. Garralon, G., Carma, A., and Fornes, V., *Zeolites* **9,** 84 (1989).
21. Goovaerts, F., Vansant, E. F., Philippaerts, J., DeHulsters, P., and Gelan, J., *J. Chem. Soc., Faraday Trans. 1* **85**(11), 3675 (1989).
22. Hopkins, P. D., Marshall, C. L., Miller, J. T., and Raska, L. B., *in* "Catalysis 1987" (J. W. Ward, Ed.), p. 281. Elsevier, Amsterdam, 1988.
23. Wang, I., Chen, T.-J., Chao, K.-J., and Tsai, T.-C., *J. Catal.* **60,** 140 (1979).
24. Meyers, B. L., Fleisch, T. H., Ray, G. J., Miller, J. T., and Hall, J. B., *J. Catal.* **110,** 82 (1988).
25. Karge, H. G., Dondur, V., and Weitkamp, J., *J. Phys. Chem.* **95,** 283 (1991).
26. Ma, Y. A., and Ho, S. Y., *AIChE J.* **20,** 279 (1974).
27. Weisz, P. B., and Miale, J. N., *J. Catal.* **4,** 527 (1965).
28. Miale, J. N., Chen, N. Y., and Weisz, P. B., *J. Catal.* **6,** 278 (1966).
29. Engelhardt, G., and Michel, D., "High Resolution Solid-State NMR of Silicates and Zeolites," p. 150. Wiley, New York, 1987.
30. Ripmeester, J. A., Majid, A., and Hawkins, R. E., *J. Inclusion Phenom.* **1,** 193 (1983).
31. Hays, G. R., Van Erp, W. A., Alma, N. C. M.,

Couperus, P. A., Huis, R., and Wilson, A. E., *Zeolites* **4,** 377 (1984).
32. Engelhardt, G., Lohse, U., Samoson, A., Magi, M., Tarnak, M., and Lippmaa, E., *Zeolites* **2,** 59 (1982).
33. Hunger, M., Karger, J., Pfeifer, H., Caro, J., Zibrowius, B., Bulow, M., and Mostowicz, R., *J. Chem. Soc., Faraday Trans 1* **83,** 3459 (1987).
34. Chen, N. Y., and Smith, F. A., *Inorg. Chem.* **15,** 295 (1976).
35. Lippmaa, E., Samoson, F. A., and Magi, M., *J. Am. Chem. Soc.* **108,** 1730 (1986).
36. Klinowski, J., Thomas, J. M., Fyfe, C. A., and Gobbi, G. C., *Nature (London)* **296,** 533 (1982).
37. Gilson, J.-P., Edwards, G. C., Peters, A. W., Rajagopalan, K., Wormsbecher, R. F., Roberie, T. G., and Shatlock, M. P., *J. Chem. Soc., Chem. Commun.,* 91 (1987).
38. Samoson, A., Lippmaa, E., Engelhardt, G., Lohse, U., and Jerschkewitz, H.-G., *Chem. Phys. Lett.* **134,** 589 (1987).
39. Ray, G. J., Meyers, B. L., and Marshall, C. L., *Zeolites* **7,** 307 (1987).
40. Sanz, J., Fornes, V., and Corma, A., *J. Chem. Soc., Faraday Trans 1* **84,** 3113 (1988).
41. Grobert, P. J., Geerts, H., Martens, J. A., and Jacobs, P. A., *J. Chem. Soc., Chem. Commun.,* 1688 (1987).
42. Basil, M. R., Kantner, T. R., and Rhee, K. H., *J. Phys. Chem.* **68,** 3197 (1964).
43. Lefrancois, M., and Malbois, G., *J. Catal.* **20,** 350 (1971).
44. Rhee, K. H., Udaya, V., Roa, S., Stencel, J. M., Melson, G. A., and Crawford, J. E., *Zeolites* **3,** 337 (1983).
45. Ripmeester, J. A., *J. Magn. Reson.* **56,** 247 (1984).
46. Ito, T., and Fraissard, J., *J. Chem. Phys.* **76,** 5225 (1982).
47. Fraissard, J., Ito, T., Springuel-Huet, M., and Demarquay, J., *Stud. Surf. Sci. Catal.* **28,** 393 (1986).
48. Cvetanovic, R. J., and Amenomiya, Y., *Adv. Catal.* **17,** 103 (1967).
49. Topsoe, N.-Y., Pedersen, K., and Derouane, E. G., *J. Catal.* **70,** 41 (1981).
50. Post, J. G., and van Hooff, J. H. C., *Zeolites* **4,** 9 (1984).
51. Sawa, M., Niwa, M., and Murakami, Y., *Zeolites* **10,** 307 (1990).
52. Sawa, M., Niwa, M., and Murakami, Y., *Zeolites* **11,** 93 (1991).
53. Fleisch, T. H., Ray, G. J., Meyers, B. L., and Marshall, C. L., *J. Catal.* **99,** 117 (1986).
54. Cotterman, R. L., Hicksen, D. A., Cartlidge, S., Dybowski, C., Tsao, C., and Venaro, A. F., *Zeolites* **11,** 27 (1991).